Vietnam Journal of Science and Technology ***59*** *(3) (2021) 277-289*

doi:10.15625/2525-2518/59/3/15490

ON THE CONTRIBUTION FACTORS OF ENHANCED PHOTOCATALYTIC ACTIVITY OF DOPED SEMICONDUCTORS: STRUCTURAL AND OPTICAL INTVESTIGATION OF Cu^{2+} DOPED ZnO NANOPARTICLES

Ta Duy Quynh[1], Luu Thi Lan Anh[2], Nguyen Xuan Sang[1,*]

[1]*Saigon University, 273 An Duong Vuong, Ward 3, District 5, Ho Chi Minh City, Viet Nam*

[2]*School of Engineering Physics, Hanoi University of Science and Technology, 1 Dai Co Viet, Ha Noi, Viet Nam*

[*]Email: *sangnguyen@sgu.edu.vn*

Received: 13 September 2020; Accepted for publication: 2 March 2021

Abstract. This work studied the photocatalytic activity improvement of ZnO doped with Cu^{2+} ion and tried to illustrate the crucial photocatalytic enhancement factors. The structural and morphological properties of synthesized materials were characterized by X-ray diffractometry (XRD), Raman spectroscopy, and transmission electron microscopy (TEM). It showed that the crystal lattice parameters of ZnO were not affected by the doping manner. However, the crystallite size was slightly decreased in the doped sample. Furthermore, the visible photocatalytic activity of the doped sample was enhanced in comparison with that of the undoped ZnO, so that the reaction rate constants of ZnO and ZnO:Cu were 0.00528 and 0.00968 min^{-1}, respectively. This work also showed that narrowing bandgap did not contribute into the enhanced photocatalytic activity rather than visible light absorption capacity and recombination rate.

Keywords: doped ZnO nanoparticle, photocatalysis, bandgap, recombination rate, visible absorption.

Classification numbers: 2.1.1, 2.4.2, 2.5.1.

1. INTRODUCTION

Nowadays, photocatalytic activity of photocatalysts towards the degradation of organic compounds has been widely investigated. Among many studies on semiconductors as potential photocatalysts, researches on ZnO - an excellent photocatalyst candidate - are of great interest thanks to its own characteristics as a cheap, non-toxic, and environmentally friendly material. Further studies on ZnO as a direct wide-bandgap semiconductor (E_g ~ 3.37 eV) with large exciton binding energy (60 meV at room temperature) should be carried out in advance, as compared to photocatalytic application [1]. For increasing the visible-light harvesting, bandgap engineering should be applied to decrease the ZnO bandgap and/or introduce defect states in the bandgap [2]. Furthermore, the decrease of recombination rate of electron-hole pair is an important task to be carried out with this material, especially to avoid its large exciton binding energy. Hence, previous reports showed that the photocatalytic activity of ZnO was enhanced by

compositing with other semiconductors [3, 4], carbon-based materials [5, 6], or by doping with other metal and non-metal ions [7 - 9]. These experiments were targeted to form a heterojunction of the semiconductor host and the other materials which have showed advantages in photocatalytic enhancement in many studies. However, the contribution of the enhancement factors due to the heterojunction formation, i.e. bandgap reduction, improved visible-light harvesting, and prolonged recombination rate, was not clearly illustrated.

In this work, we have proposed a simple method to enhance the photocatalytic activity of ZnO nanoparticles fabricated by sol-gel method in which Cu^{2+} ion, a transition metal ion, was used for *in-situ* ZnO doping. UV and visible photocatalytic activities were characterized by decolorisation of methylene blue (MB). Moreover, this work has also attempted to illustrate the important factors which contribute to enhanced photocatalytic activity by characterising the optical properties from experimental photoluminescence emission and UV-vis diffuse reflectance spectra.

2. MATERIALS AND METHODS

The $Zn_{1-x}Cu_xO$ samples with x = 0.0 and 0.01 were prepared by sol-gel method similar to previous reports [10, 11]. Typically, the zincnitratehexahydrate – $Zn(NO_3)_2.6H_2O$ (Sigma-Aldrich) and copper(II) nitrate trihydrate – $Cu(NO3)_2.3H_2O$ (Sigma-Aldrich) were mixed with citric acid – $C_6H_8O_7.H_2O$ 1M (Sigma-Aldrich) with a molar ratio of metal ions : acid = 1:3. The resulted solution was stirred at 80 ^oC for 1 h, then heated at 150 ^oC for 4 hto form a powder. After that, the powder was annealed at 400 ^oC for 4 h in air. The undoped and doped samples were named as ZnO and ZnO:Cu, respectively.

Structural and morphological properties were determined using a Bruker D8 Advance X-ray diffractometry (XRD) with a CuKα radiation source (λ = 1.54064 Å) and a sweep range 2θ of 20^o - 70^o. Optical bandgap was determined by UV–Vis absorption measurement using UV–Vis spectrophotometry (Metash, UV-S100). The photoluminescence emission characteristics were recorded at room temperature by an analog spectrophotometer (Horiba, JobinYvon) equipped with a Xe lamp as an excitation source at a wave length of 325 nm. Photocatalytic activities were investigated by UV–Vis spectrophotometry (Metash, UV-S100) by determining the degradation of methylene blue in solution under simulated ultraviolet (UV) and natural visible light irradiation.

3. RESULTS AND DISCUSSION

3.1. Phase and structure

Figure 1a showed XRD patterns of ZnO and ZnO:Cu. The main diffraction peaks in the XRD patterns of these samples are indexed according to the wurtzite structure (hexagonal) of ZnO at diffraction angles (2θ) of 31.5^o, 34.12^o, 35.97^o, 47.28^o, 56.38^o, 62.62^o, 66.19^o, 67.74^o, 68.90^o corresponding to faces of (100), (002), (101), (102), (110), (103), (200), (112) and (201), respectively (JCPDS 36-1451) [12]. As can be seen from the XRD of ZnO:Cu sample, there is no extra peaks related to the impurity of an external phase. Figure 1b showed the micrograph of the undoped ZnO, whereby the nanoparticles were fairly uniform in spherical morphology shape with a diameter of ~20 - 25 nm.

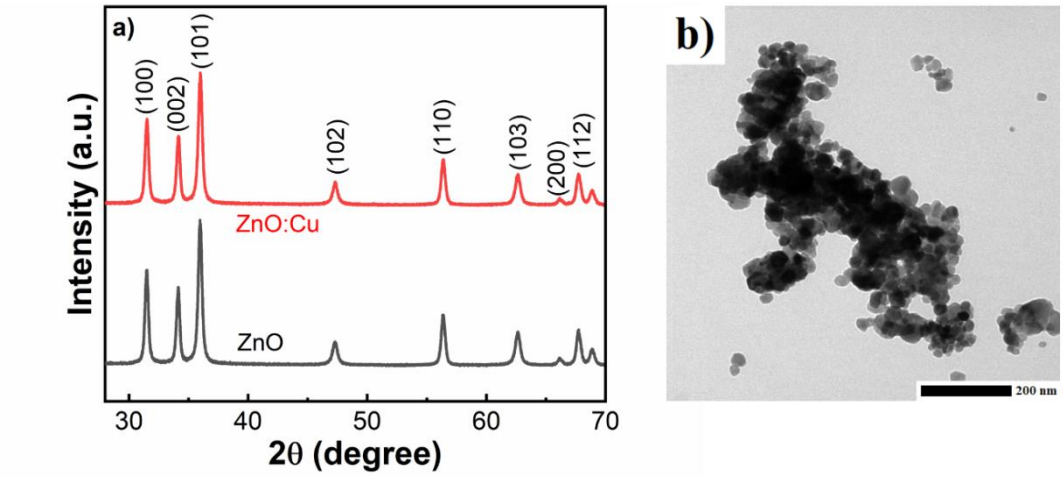

Figure 1. a) XRD patterns of ZnO and ZnO:Cu samples and b) TEM image of pure ZnO sample.

In order to study the effect of the dopant on the crystal structure of the host, lattice parameters (*a* and *c*), crystallite size and d-spacing distance should be identified. The lattice parameter could be obtained by Bragg's law:

$$2d_{hkl}\sin\theta = n\lambda \ \ where\ n = 1, 2, ... \tag{1}$$

where d_{hkl} is the spacing distance of two consecutive planes in the same direction; h, k, l are Miller indexes; n = 1; λ is the wavelength of incident X-ray 1.5406 Å. Then the lattice constants of the wurtzite structure (hexagonal) of ZnO could be calculated using the following equation [13]:

$$\frac{1}{d_{hkl}^2} = \frac{4}{3}\left(\frac{h^2 + hk + k^2}{a^2}\right) + \frac{l^2}{c^2} \tag{2}$$

The crystallite size can be calculated by using Debye-Scherrer method as follows:

$$D = \frac{0.89 \times \lambda}{\beta \times \cos\theta} \tag{3}$$

where D, λ, β and θ are respectively crystallite size (nm), wavelength of incident X-ray (nm), full-widthhalf-maximum–FWHM (degree), diffraction angle (degree), and 0.89 is the Debye-Scherrer effective constant. The crystallite size calculated is given in Table 1. The average crystallite size, lattice parameters, d-spacing distance were then calculated and shown in Table 2. It is clear that the d-spacing distance (~0.249 nm) and the lattice parameters (a ~ 0.327 and c ~ 0.523 nm) of ZnO and ZnO:Cu were similar, indicating that Cu^{2+} dopant did not affect ZnO lattice. However, the average crystallite size of the doped sample (~19.77 nm) was slightly decreased in comparison to that of the pure ZnO (~ 20.68 nm). To further study the doping effect on crystallite ZnO structure, a modified Williamson-Hall (W-H) method with uniform deformation model (UDM) was applied [5, 14, 15]. We started at the following equation [16]:

Table 1. The crystallite size of undoped ZnO and ZnO:Cu samples obtained using Debye-Scherrer equation.

Sample	Crystal lattice	FWHM (Rad)	Crystallite size (nm)	Correlation parameter (R^2)	Average crystallite size (nm)
ZnO	(100)	0.006324	22.53	0.99052	20.46
	(002)	0.005964	24.05	0.99170	
	(101)	0.006924	20.82	0.99140	
	(102)	0.009155	16.35	0.98228	
	(110)	0.007265	21.41	0.99386	
	(103)	0.009114	17.61	0.98895	
ZnO:Cu	(100)	0.006525	21.83	0.99272	19.77
	(002)	0.006119	23.44	0.99223	
	(101)	0.007331	19.66	0.98976	
	(102)	0.009514	15.73	0.97900	
	(110)	0.007445	20.90	0.99419	
	(103)	0.009398	17.08	0.98811	

Table 2. The d-spacing, lattice parameter, average crystallite size of undoped ZnO and ZnO:Cu samples.

Sample	d_{101} (nm)	*a* (nm)	*c* (nm)	Average crystallite size (nm)
ZnO	0.2495	0.3277	0.5235	20.68
ZnO:Cu	0.2493	0.3275	0.5229	19.77

$$\beta \cos\theta = 2\varepsilon \sin\theta + \frac{0.9\lambda}{D} \quad (4)$$

where β, θ, λ, and ε are full-widthhalf-maximum–FWHM (degree), diffraction angle (degree), wavelength of incident X-ray (nm), and microstrain, respectively. Equation (4) is a linear equation that can be written as y = ax + b; where y-axis (βcosθ) and x-axis (2sinθ) were determined by diffraction peaks of the synthesized samples. The average crystallite size and the microstrain could be estimated by a linear fitting as shown in Fig. 2. The crystallite size and microstrain were calculated and given in Table 3.

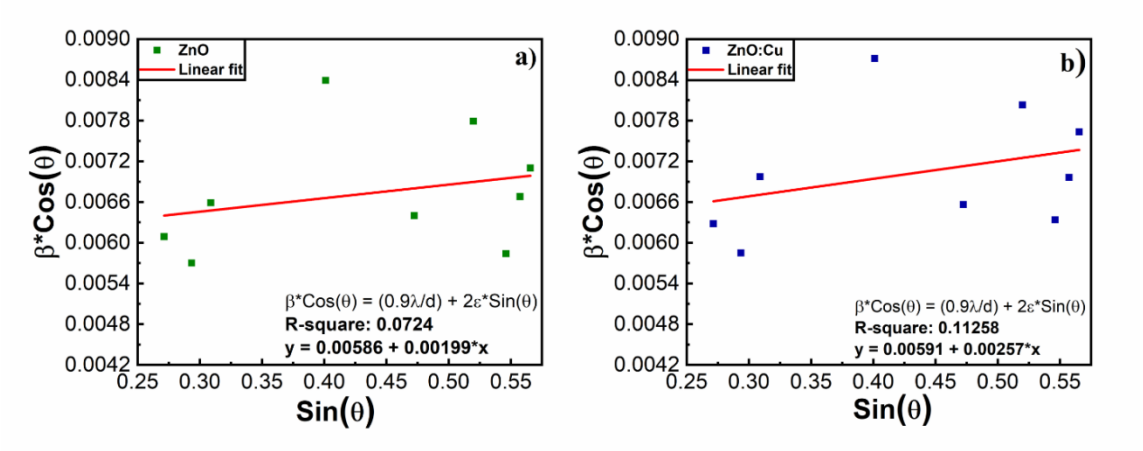

Figure 2. Williamson–Hall analysis of samples a) ZnO and b) ZnO:Cu.

Table 3. The average crystallite size, microstrain of undoped ZnO and ZnO:Cu samples obtained using W-H method.

	Intercept	Average crystallite size (nm)	Microstrain ($\times 10^{-4}$)	Wavelength (nm)
ZnO	0.00586	23.66	9.95	0.15406
ZnO:Cu	0.00591	23.46	12.85	0.15406

The average crystallite size of ZnO and ZnO:Cu calculated by W-H method was in good agreement with the result obtained by Derbye-Scherrer method, the crystallite size was slightly decreased in the doped sample. Furthermore, the microstrain obtained by W-H method in the doped sample was decreased showing that Cu^{2+} ions could diffuse into ZnO lattice to reduce its surface energy. However, the correlation parameter (R^2) was low indicating that this method is not good to apply. As reported in the literature, W-H method could only have a high R^2 value when the nanocrystallite size was larger than 35 nm [5, 14, 15].

3.2. Photocatalytic activity experiment

The photocatalytic activity of synthesized samples was tested by measuring the decomposition of methylene blue (MB) dye under both UV and visible light irradiation [17]. A sample of 0.02 g was magnetically stirred in 250 mL of a solution containing methylene blue at a concentration of 25 ppm in dark for 60 min in order to obtain the equilibrium state of the absorption, and then the mixed solution was irradiated under UV light or solar light for photocatalytic experiments. The optical investigations were performed with UV–Vis spectrophotometry in a wavelength sweep range of 250 - 800 nm.

Figure 3 shows UV-vis absorption spectra of ZnO and ZnO:Cu samples indicating the degradation of MB under UV irradiation, whereby the MB degradation efficiency of the doped ZnO was higher than that of the undoped ZnO. The efficiency of photocatalytic MB decomposition was calculated by comparing the decrease of MB at its characteristic absorption peak (664 nm) shown in Fig. 4. At the end of the photocatalytic reaction, MB degradation efficiencies of ZnO and ZnO:Cu samples were 3.48 % and 17.41 %, respectively.

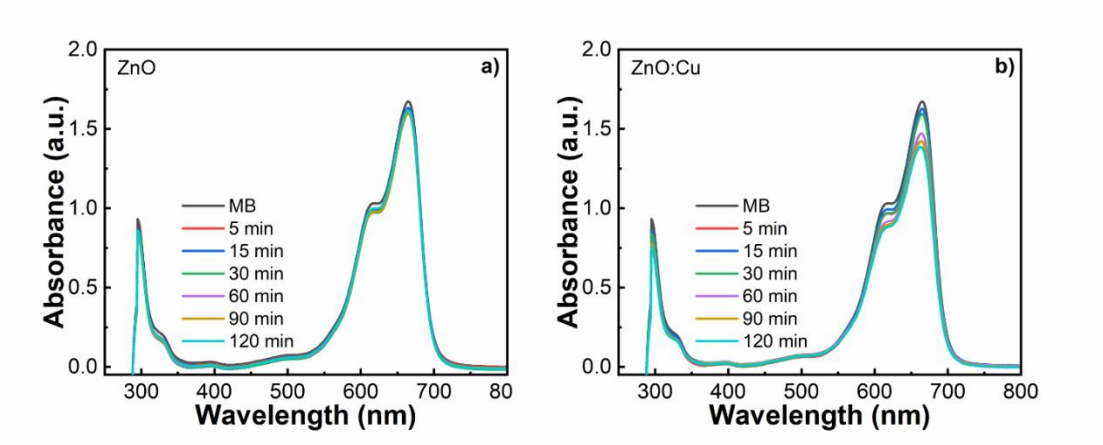

Figure 3. UV irradiation induced MB degradation characterized by UV-vis absorption spectra of a) undoped ZnO and b) ZnO:Cu samples.

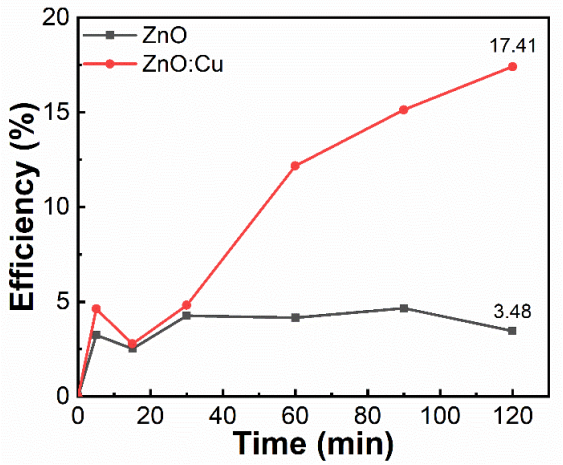

Figure 4. The UV photocatalytic efficiency of MB degradation of the undoped and doped ZnO samples.

It can be seen that the performance of ZnO:Cu samples is higher than that of pure ZnO, however the efficiencies of both samples were quite low. We then carried out the photocatalytic measurement under solar light irradiation. Figure 5 showed the photocatalytic activity of ZnO and ZnO:Cu samples under visible light irradiation on a sunny day from 8 am to 11 am [18].

It can be seen from Fig. 5a) and 5b) that the intensities of absorption spectra were decreased as the irradiation time increased up to 150 min. The intensity of the MB characteristic peak at ~ 664 nm was decreased due to the degradation of methylene blue dye [17] and the degradation efficiency of the ZnO:Cu sample was better than that of the pure ZnO. Fig. 5c) shows the photocatalytic efficiency for MB degradation of the synthesized samples over time. After 150 min of exposure to visible light, the MB degradation efficiencies were about 54.95 % and 76.65 % for ZnO and ZnO:Cu, respectively. The doping effect on the enhanced photocatalytic activity could be from various reasons such as ZnO bandgap reduction [19], enhanced light absorption [20], and excited carriers separation [11] which all affect photoelectron-hole generation/recombination processes.

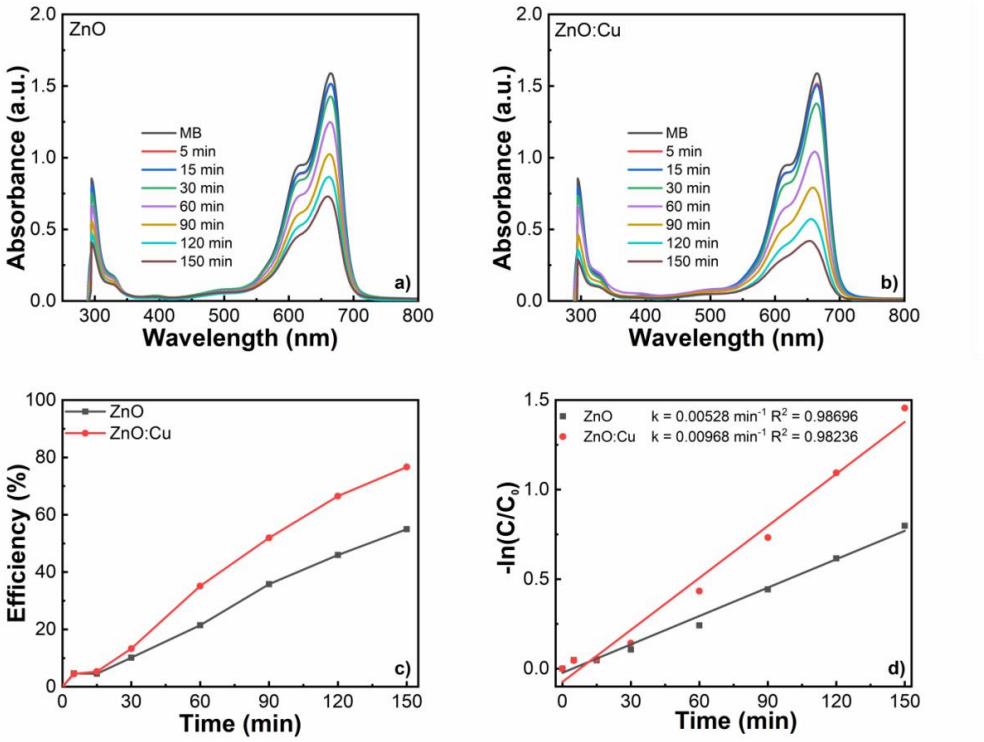

Figure 5. Sequence of MB degradation over time of a) ZnO, and b) ZnO:Cu; c) MB degradation collected at 664 nm, the MB characteristic absorption peak, and d) Pseudo-first-order model for MB degradation.

The Cu^{2+} ion dopant and donor states (oxygen vacancies/defects) act like a sink to electron and hole pairs, decreasing the electron–hole pair recombination that may lead to an increase in the production of high reactive radicals, $^{\bullet}OH$ and $^{\bullet}O_2^-$ [21] which play an important role in the photocatalytic enhancement. The overall steps of the photocatalysis process could be described as follows [22]:

$$ZnO \xrightarrow{h\nu} e_{cb}^- + h_{vb}^+ \quad \text{(i)}$$

$$e_{cb}^- + O_2 \longrightarrow {}^{\bullet}O_2^- \quad \text{(ii)}$$

$$h_{vb}^+ + OH^- \longrightarrow {}^{\bullet}OH \quad \text{(iii)}$$

$$Cu^+ + H_2O_2 \rightarrow Cu^{2+} + OH^- + {}^{\bullet}OH \quad \text{(iv)}$$

$$Cu^{2+} + e^- \rightarrow Cu^+ \quad \text{(v)}$$

$${}^{\bullet}OH + \text{MB (dye)} \rightarrow CO_2 + H_2O + \text{other inorganic products} \quad \text{(vi)}$$

$${}^{\bullet}O_2^- + \text{MB (dye)} \rightarrow CO_2 + H_2O + \text{other inorganic products} \quad \text{(vii)}$$

The photocatalytic decomposition of methylene blue dye of the synthesized samples also follows the pseudo-first-order kinetic model [23 - 26], which can be expressed as:

$$r = -\frac{dC}{dt} = Kt \quad (8)$$

Taking integral ofequation (8):

$$\ln\left(\frac{C_0}{C}\right) = Kt \rightarrow K = \frac{1}{t}\ln\frac{C_0}{C_t} \quad (9)$$

where C and C_0 are the methylene blue concentrations at time t = t and t = 0, respectively; K and t are the pseudo-first-order rate constant (reaction rate constant) and time, respectively; the relationship between $\ln(C_t/C_0)$ and irradiation time is shown in Fig. 5d.

The obtained pseudo-first-order rate constant (K) and linear correlation coefficient (R) were summarized in Table 4. It showed that the photoreaction rate of the doped ZnO was higher than that of the pure ZnO, i.e. ~ 5.28×10^{-3} and ~9.68×10^{-3} min^{-1} for ZnO and ZnO:Cu, respectively. In order to understand the insights of the photocatalytic enhancement, optical properties of the synthesized samples were determined, which will be discussed in the next section.

Table 4. Reaction rate constants of ZnO and ZnO:Cu samples.

Experiment	Sample	$K(min^{-1})$	R^2
1	ZnO	0.00528	0.98882
2	ZnO:Cu	0.00968	0.98488

3.3. Optical properties

a) Photoluminescence (PL) emission

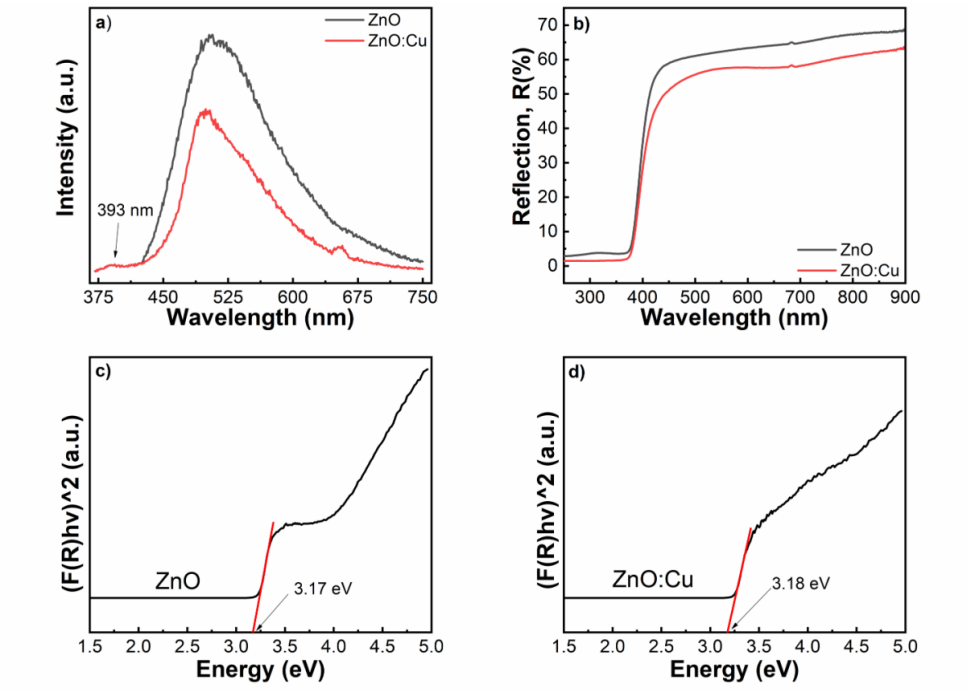

Figure 6.a) Photoluminescence spectra; b) DRS; c) and d) Bandgap energy E_g for undoped ZnO and ZnO:Cu samples by Tauc's plot method, respectively.

Photoluminescence (PL) emission is a suitable and nondestructive technique to determine the emissions assigned to radiative recombinations of electron-hole pairs in semiconductors and the presence of impurities and point defects. In principle, the PL peak in UV range is associated to the near band-to-band emission (NBE) while the visible emission range originates from the defects, which includes zinc vacancies (V_{Zn}), interstitial zinc (Zn_i), interstitial oxygen (O_i) and lattice defects relating to oxygen and zinc [27]. Figure 6a showed room temperature PL spectra of the synthesized samples.

For both samples, a broad intense deep-level (DL) emission appears in a range of 400 - 750 nm. In general, the PL emission intensity of the ZnO:Cu was lower than that of the pure ZnO indicating that the radiative recombination rate was decreased in the doped sample. Hence the lifetimes of carriers, photoelectron and hole, were prolonger when introducing Cu^{2+} ions into the ZnO host, thus these reactive centers could have more time to decompose methylene blue to enhance the photocatalytic activity.

b) UV-vis diffuse reflectance spectroscopy (DRS)

UV-vis DRS of the synthesized samples shown in Fig. 6b indicatesthat the ZnO:Cu sample absorbed visible light better than the undoped ZnO sample. Hence, the increase of the light absorption capacity in the ZnO:Cu sample could be a good reason for enhancing the photocatalytic activity. Furthermore, the DRS of the doped sample shifted to the longer wavelength compared to the pure ZnO which can lead to the bandgap reduction, promoting the doped sample to absorb more visible light and thus, to improve the visible photocatalytic ability [18]. For further investigation of the bandgap value of the synthesized samples, the extrapolated method was applied to determine the bandgap value through Tauc's plot for the direct ZnO bandgap by the following equation:

$$\alpha h\nu = A(h\nu - E_g)^n \tag{10}$$

where n is type of optical transition, α and *A* are absorption coefficient and optical transition-dependent constant, hυ andE_g are the energy of the photon and the band gap energy, respectively. In this case, ZnO is a direct wide-bandgap semiconductor, therefore the value of the optical transition n is ½ (plotted as $a(h\upsilon)^2$ versus E) [28]. Figures 6c and 6d showed the bandgap values of ZnO and ZnO:Cu, respectively, whereby the bandgap estimated for pure ZnO (3.17 eV) isalmost the same as for ZnO:Cu (3.18 eV), which contradicts previous reports of the doped ZnO studies [29, 30].

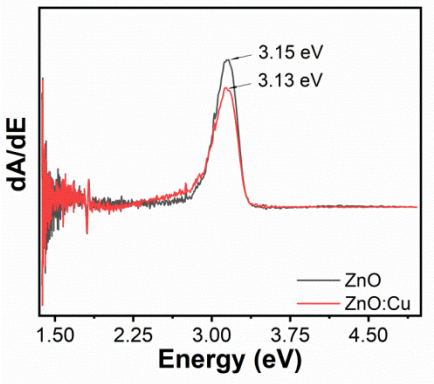

Figure 7. Bandgap energy E_g for undoped ZnO and ZnO:Cu samples by first derivative method.

We then used the first derivative method to obtain the bandgap of the synthesized powders [31] as given in Fig. 7. The result showed that the bandgaps obtained by the first derivative method were similar to Tauc's plot method, i.e. 3.15 eV and 3.13 eV for ZnO and ZnO:Cu samples, respectively. It could be stated that the doping manner did not change the bandgap value of ZnO. Many ZnO photocatalytic studies have concluded that the reduction of bandgap in the doped ZnO nanostructure results in improved photocatalytic activity. In this case, however, it can be seen that the bandgap reduction was insignificant and not the matter of enhanced photocatalytic activity. The enhancement of the photocatalytic activity in the doped sample could be from improving light harvesting and lowering recombination rate in the doped sample. Furthermore, their values were remained in UV-region.

4. CONCLUSIONS

This work has studied the photocatalytic improvement of ZnO doped with Cu^{2+} ions in the degradation of methylene blue in both UV and visible range. The ZnO nanoparticle and its Cu-doped material were synthesized by a facile sol-gel method giving a homogeneous particle size of ~ 20 nm which was in agreement with Scherrer-Debye and W-H calculations. Furthermore, we have showed that the bandgap narrowing obtained from doping was not a major factor in the photocatalytic improvement. The increase of visible-light absorption and the decrease in recombination rate are attributed to the photocatalytic enhancement.

Acknowledgement This research is funded by Vietnam National Foundation for Science and Technology Development (NAFOSTED) under grant number 103.02-2019.362.

CRediT authorship contribution statement. Ta Duy Quynh: Experimental, Data curation, Investigation, Writing original draft. Luu Thi Lan Anh: Formal analysis, methodology, data curation. Nguyen Xuan Sang: Conceptualization, Formal analysis, Writing original draft, Supervision, Funding acquisition.

Declaration of competing interest. The authors declare that they have no known competing financial interests or personal relationships that could have appeared to influence the work reported in this paper.

REFERENCES

1. Khaki M. R. D., Shafeeyan M. S., Raman A. A. A., and W. Daud M. A. - Application of doped photocatalysts for organic pollutant degradation - A review. J. Environ Manage **198** (Pt 2) (2017) 78-94 https://10.1016/j.jenvman.2017.04.099.
2. Bora T., Sathe P., Laxman K., Dobretsov S., and Dutta J. - Defect engineered visible light active ZnO nanorods for photocatalytic treatment of water, Catalysis Today **284** (2017) 11-18 https://doi.org/10.1016/j.cattod.2016.09.014.
3. Hou T. F., Shanmugasundaram A., Hassan M. A., Johar M. A., Ryu S. W., and Lee D. W. - ZnO/Cu_2O-decorated rGO: Heterojunction photoelectrode with improved solar water splitting performance, International Journal of Hydrogen Energy **44** (2019) 19177-19192 https://doi.org/10.1016/j.ijhydene.2018.05.105.
4. Ko Y. C., Fang H. Y., and Chen D. H. - Fabrication of Ag/ZnO/reduced graphene oxide nanocomposite for SERS detection and multiway killing of bacteria, Journal of Alloys and Compounds **695** (2017) 1145-1153 https://doi.org/10.1016/j.jallcom.2016.10.241.
5. Pham V. T., Tran T. P., Vu T. T., Nguyen X. S., and Tran N. K. - In-situ hydrothermal fabrication and photocatalytic behavior of ZnO/reduced graphene oxide nanocomposites

with varying graphene oxide concentrations, Materials Science in Semiconductor Processing **115** (2020) 105114 https://doi.org/10.1016/j.mssp.2020.105114.

6. Raizada P., Sudhaik A., Singh P. - Photocatalytic water decontamination using graphene and ZnO coupled photocatalysts: A review, Materials Science for Energy Technologies **2** (2019) 509-525 https://doi.org/10.1016/j.mset.2019.04.007.
7. Choi S., Do J. Y., Lee J. H., Ra C. S., Kim S. K., and Kang M. - Optical properties of Cu-incorporated ZnO (Cu x Zn y O) nanoparticles and their photocatalytic hydrogen production performances, Materials Chemistry and Physics **205** (2018) 206-209 https://doi.org/10.1016/j.matchemphys.2017.11.022.
8. Achouri F., Corbel S., Balan L., Mozet K., Girot E., Medjahdi G., Said M. B., Ghrabi A. and Schneider R. - Porous Mn-doped ZnO nanoparticles for enhanced solar and visible light photocatalysis, Materials & Design **101** (2016) 309-316.

   https://doi.org/10.1016/j.matdes.2016.04.015.
9. Janisch R., Gopal P., Spaldin N. - Transition metal-doped TiO_2 and ZnO-present status of the field, Journal of Physics: Condensed Matter. **17** (2005) R657-R689 https://doi.org/10.1088/0953-8984/17/27/r01.
10. Nguyen X. S., Nguyen M. Q., Trinh X. T., Joita A. C., and Nistor S. V. - Correlation of native point defects and photocatalytic activity of annealed ZnO nanoparticle studied by electron spin resonance and photoluminescence emission, Semiconductor Science and Technology **35** (2020) 095035 https://doi.org/10.1088/1361-6641/aba168.
11. Nguyen X. S., Nguyen M. Q., Nguyen H. T., Nguyen T. T., and Tran T. T. - Mechanism of enhanced photocatalytic activity of Cr-doped ZnO nanoparticles revealed by photoluminescence emission and electron spin resonance, Semiconductor Science and Technology **34** (2019) 025013 https://doi.org/10.1088/1361-6641/aaf820.
12. Luo X., Lee W. T., Xing G., Bao N., Yonis A., Chu D., Lee J., Ding J., Li S., and Yi J. - Ferromagnetic ordering in Mn-doped ZnO nanoparticles, Nanoscale Research Letters, **9**:625 (2014).
13. Iqbal A., Mahmood A., Khan T. M., and Ahmed E. - Structural and optical properties of Cr doped ZnO crystalline thin films deposited by reactive electron beam evaporation technique, Progress in Natural Science: Materials International **23** (2013) 64-69 https://doi.org/10.1016/j.pnsc.2013.01.010.
14. Nguyen C. T., Pham T. P., Luu T. L. A., Nguyen X. S., Nguyen T. T., Nguyen H. L., and Nguyen D. C. - Constraint effect caused by graphene on in situ grown Gr@WO3 - nanobrick hybrid material, Ceramics International **46** (2020) 8711-8718 https://doi.org/10.1016/j.ceramint.2019.12.108.
15. Nath D., Singh F., and Das R. - X-ray diffraction analysis by Williamson-Hall, Halder-Wagner and size-strain plot methods of CdSe nanoparticles- a comparative study, Materials Chemistry and Physics **239** (2020) 122021.

   https://doi.org/10.1016/j.matchemphys.2019.122021.
16. Safa S., Azimirad R., Moghaddam S. S., and Rabbani M. - Investigating on photocatalytic performance of CuO micro and nanostructures prepared by different precursors, Desalination and Water Treatment **57** (2015) 6723-6731.

   https://doi.org/10.1080/19443994.2015.1012561.

17. Sang N. X., Huong P. T. L., Thy T. T. M., Dat P. T., Minh V. C., Tho N. H. - Crystalline deformation and photoluminescence of titanium dioxide nanotubes during in situ hybridization with graphene: An example of the heterogeneous photocatalyst, Superlattices and Microstructures **121** (2018) 9-15.

    https://doi.org/10.1016/j.spmi.2018.07.020.

18. Sang N. X., Minh V. C. - Thermal annealing-induced self-junction of hydrothermal titanate nanotubes/TiO2 nanoparticles with enhanced photocatalytic activity, Nanotechnology **31** (2020) 435703 https://doi.org/10.1088/1361-6528/aba65c.

19. Qamar M. A., Shahid S., Javed M., Iqbal S., Sher M. and Akbar M. B. - Highly efficient g-C3N4/Cr-ZnO nanocomposites with superior photocatalytic and antibacterial activity, Journal of Photochemistry and Photobiology A: Chemistry **401** (2020) 112776 https://doi.org/10.1016/j.jphotochem.2020.112776.

20. Manzoor M. F., Ahmed E., Ahmad M., Ahmad I. A., Rana A. M., Absar Ali A., Ghouri M. I., Manzoor M. S. and Aziz M. T. - Enhanced photocatalytic activity of hydrogen evolution through Cu incorporated ZnO nano composites, Materials Science in Semiconductor Processing **120** (2020) 105278.

    https://doi.org/10.1016/j.mssp.2020.105278.

21. Okamato K., Yamamoto Y., Tanaka H., Tanaka M., Itaya A. - Heterogeneous Photocatalytic Decomposition of Phenol over TiO_2 Powder, The Chemical Society of Japan **58** (1985) 2015-2022.

22. Carvalho H. W. P., Batista A. P. L., Hammer P. and Ramalho T. C. - Photocatalytic degradation of methylene blue by TiO2-Cu thin films: theoretical and experimental study, J. Hazard Mater. **184** (2010) 273-280 https://doi.org/10.1016/j.jhazmat.2010.08.033.

23. Sang N. X., Quan N. M., Tho N. H., Tuan N. T. and Tung T. T. - Mechanism of enhanced photocatalytic activity of Cr-doped ZnO nanoparticles revealed by photoluminescence emission and electron spin resonance, Semiconductor Science and Technology **34** (2019) https://doi.org/10.1088/1361-6641/aaf820.

24. Rupa A.V., Manikandan D., Divakar D. and Sivakumar T. - Effect of deposition of Ag on TiO2 nanoparticles on the photodegradation of Reactive Yellow-17, J. Hazard Mater. **147** (2007) 906-913 https://doi.org/10.1016/j.jhazmat.2007.01.107.

25. Xu J., Ao Y., Fu D. and Yuan C. - Low-temperature preparation of F-doped TiO2 film and its photocatalytic activity under solar light, Applied Surface Science **254** (2008) 3033-3038 https://doi.org/10.1016/j.apsusc.2007.10.065.

26. Wu L., Yan H., Xiao J., Li X., Wang X., Zhao T. - Characterization and photocatalytic properties of nano-Fe2O3–TiO2 composites prepared through the gaseous detonation method, Ceramics International **43** (2017) 14334-14339.

    https://doi.org/10.1016/j.ceramint.2017.07.189.

27. Sang N. X., Sang L. P., Quan N. M., and Tho N. H. - Photoluminescence and point defect related emission of $ZnO:Mn^{2+}$ micro/nanorod fabricated by co-precipitation method, VNU Journal of Science: Mathematics - Physics **34** (2018) https://doi.org/10.25073/2588-1124/vnumap.4273.

28. López R. and Gómez R. - Band-gap energy estimation from diffuse reflectance measurements on sol–gel and commercial TiO_2: a comparative study, Journal of Sol-Gel Science and Technology **61** (2011) 1-7 https://doi.org/10.1007/s10971-011-2582-9.

29. Priyadharsan A., Shanavas S., Vidya C., Kalyana Sundar J., Acevedo R. and Anbarasan P. M. - Structural and optical properties of Sn doped ZnO-rGO nanostructures using hydrothermal technique, Materials Today: Proceedings (2019).

    https://doi.org/10.1016/j.matpr.2019.05.440.

30. Kang W., Jimeng X. and Xitao W. - The effects of ZnO morphology on photocatalytic efficiency of ZnO/RGO nanocomposites, Applied Surface Science **360** (2016) 270-275 https://doi.org/10.1016/j.apsusc.2015.10.190.

31. Phan T. D., Vo C. M., Tran T. M. T., Luu T. L. A., and Nguyen X. S. - Structural and bandgap properties of titanium dioxide nanotube/graphene oxide composites prepared by a facile hydrothermal method, Materials Research Express **6** (2019) 105054 https://doi.org/10.1088/2053-1591/ab3a0b.